Pergamon

Int. J. Heat Mass Transfer. Vol. 38, No. 5, pp. 779–794, 1995

0017–9310/95 $9.50+0.00

0017–9310(94)00213–4

Local condensation rates of steam–air mixtures in direct contact with a falling liquid film

T. D. KARAPANTSIOS, M. KOSTOGLOU and A. J. KARABELAS†

Chemical Process Engineering Research Institute and Department of Chemical Engineering, Aristotle University of Thessaloniki, University Box 455, GR 540 06 Thessaloniki, Greece

(*Received* 3 *August* 1993 *and in final form* 16 *July* 1994)

Abstract—Local condensation heat transfer rates are measured for steam–air mixtures in direct contact with subcooled water layers inside a vertical tube over a wide range of liquid flow rates. The gas mixture is maintained effectively stagnant during the tests and the major resistance to heat transfer is due to the large amount of noncondensables. A theoretical model is developed to account for some additional thermal resistance on the liquid side, by decomposing the liquid film into a wavy 'nonresistant' region and a substrate region where temperature gradients may prevail. Heat transfer coefficients are found to depend not only on the steam concentration but also on the liquid flow rate. Interestingly, wave characteristics of the falling liquid layer, such as the dominant wave velocity and frequency, demonstrate that condensation may only be responsible for minor modifications of the isothermal liquid surface morphology. Furthermore, the dependence of heat transfer coefficients on the liquid flow rate is attributed to the dynamic interaction between the interfacial waves and the gas layer. This notion is utilized by correlating measured gas Sherwood numbers with the gas Grashof number and a dimensionless parameter which characterizes the interface.

INTRODUCTION

Studies of direct-contact condensation are of importance for the design of equipment used in several types of industrial and power generation plants [1]. Renewed interest arises from energy transformation processes involving geothermal, solar and nuclear energy. Condensers of this type are employed because of their higher heat transfer rates, trouble-free operation and smaller initial capital outlay in comparison with the conventional indirect heat exchange equipment. A useful account on this topic has been presented by Kreith and Boehm [1].

Packed type direct-contact condensers have been recently proposed as an alternative efficient design for H_2S and CO_2 removal from geothermal steam before it enters the power generating turbines (Bontozoglou and Karabelas [2]). Structured packing is employed in the bed as it is advantageous with regard to both mass transfer and pressure drop. As Fair and Bravo [3] state, structured packings are amenable to rational modeling for predicting performance since their grooved metal surface is essentially completely wetted, and the flow over it resembles the liquid film running down a nearly vertical flat plate. Motivated by the above applications, this investigation is focused on the accurate determination of condensation heat transfer coefficients, in a falling film facility, required for the design of full-size equipment. In pursuing this goal, two important issues are addressed, i.e. the influence of noncondensable gases and the effect of waves at the gas–liquid interface on condensation rates.

A survey of the literature shows that the available data on direct contact condensation in the presence of noncondensables is scanty. Most previous studies involve pure vapor condensation on the same liquid compound or on another immiscible liquid for a wide variety of flow geometries, e.g. refs. [4–6]. Early attempts to consider the effect of noncondensables in condensation heat transfer studies are limited mostly to situations of solid wall heat transfer with relatively small amounts of noncondensables (i.e. Minkowycz and Sparrow [7]). Only recently have direct-contact condensation experiments been performed on subcooled liquid layers (i.e. Barry and Corradini [8] and Chan and Yuen [9]) in a horizontal stratified two-phase flow geometry. Even with traces of noncondensable gases present in the gas stream, the transport resistance very likely resides in the gas phase and the transport rate is no longer exclusively controlled by conditions on the liquid side. Hasson *et al.* [10] found experimentally that the average heat transfer coefficient could be reduced by up to 50% when just 1% of air was present during condensation of steam on a fan jet of water. Thus, a prime objective of this investigation is to examine the deleterious effect of relatively large amounts of noncondensables on condensation rates, shedding some light on the role of the various transport mechanisms.

With regard to the effect of interfacial waves, very little has been done when noncondensable gases are present and only for the case of thick liquid layers that

†Author to whom correspondence should be addressed.

NOMENCLATURE

A	$\lvert d^2\delta/dt^2\rvert_{mean}$, mean absolute surface acceleration [m s^{-2}]
b	apparent mass boundary layer at the gas side [m]
b'	apparent thermal boundary layer at the gas side [m]
Bo	liquid Bond number, $\rho g R^2/\sigma$, dimensionless
c_1, c_2	constants
Ca	liquid Capillary number, $\mu V_{wave}/\sigma$, dimensionless
c_p	specific heat [J kg^{-1} K^{-1}]
D	tube diameter [m]
D_g	binary mass diffusivity coefficient [m^2 s^{-1}]
D_{ii}	elements of Chebyshev–Lobatto differentiation matrix, dimensionless
g	gravitational acceleration [m s^{-2}]
Gr	gas Grashof number, $L^3 g\rho\Delta\rho/\mu^2$, dimensionless
h	condensation heat transfer coefficient [J m^{-2} s^{-1} K^{-1}]
h_g	sensible heat transfer coefficient on the gas side, k_g/b' [J m^{-2} s^{-1} K^{-1}]
k	thermal conductivity [J m^{-1} s^{-1} K^{-1}]
K_g	mass transfer coefficient on the gas side, D_g/b [m s^{-1}]
L	distance between measuring stations [m]
$\dot{m}$	cumulative condensation rate [kg s^{-1}]
p	partial pressure [Pa]
p_{am}	log mean partial pressure of noncondensable air, $(p_{as}-p_{ag})/\ln(p_{as}/p_{ag})$ [Pa]
q	local heat flux [J m^{-2} s^{-1}]
R	local radius of curvature of liquid surface, V^2_{wave}/A [equation (25)] [m]
Re	liquid Reynolds number, $4\Gamma/\mu$, dimensionless
s	standard deviation
Sh	gas Sherwood number, $K_g L/D_g$, dimensionless
Sc	gas Schmidt number, $\mu/\rho D_g$
T	temperature [K]
t	time [s]
y	distance in the radial direction [m]
u	local velocity component in the flow direction [m s^{-1}]
U_{ave}	average streamwise velocity [m s^{-1}]
V_{wave}	average streamwise wave velocity [m s^{-1}]
W	liquid flow rate [kg s^{-1}]
We	liquid Weber number, $\rho V^2_{wave} R/\sigma$, dimensionless
x	distance in the axial direction [m].

Greek symbols

α	molecular thermal diffusivity [m^2 s^{-1}]
α_e	effective thermal diffusivity [m^2 s^{-1}]
Γ	mass flow rate per unit width [kg m^{-1} s^{-1}]
δ	film thickness [m]
Θ	dimensionless temperature
λ	latent heat [J kg^{-1}]
μ	dynamic viscosity [kg m^{-1} s^{-1}]
ν	kinematic viscocity [m^2 s^{-1}]
ρ	density [kg m^{-3}]
σ	surface tension [N m^{-1}].

Subscripts

a	air
ave	average
cm	cup mixing
CUM	cumulative
g	bulk gas
i	inlet
L	local
l	liquid
min	minimum
s	surface
sub	liquid substrate
tot	total liquid
v	vapour
w	wall
wave	wave.

move in the horizontal direction (Barry and Corradini [8]) in stratified two-phase flow. In situations where the gas-phase resistance is no longer negligible (as is the case here) the transport processes are at least partly governed by the gas side conditions which, to some extent, may be dictated by the undulatory motion of the liquid–gas interface. For the purpose of this investigation, a free-falling film experimental facility was built with a vertical test section, long enough that approximately fully developed conditions could be attained by the liquid layer. The hydrodynamics of such free-falling films have already been investigated in this laboratory [11–13]. In a related piece of work, Karapantsios *et al.* [14] deal with integral-type data, corresponding to the entire test section, in the same apparatus as employed here. Useful information was obtained, concerning average heat transfer rates and the possible effect of interfacial waves, which provided the basis for designing the present experiments better. In both ref. [14] and this study, the vapour–gas mixture is maintained effectively stagnant for two reasons: first, to isolate the role played by interfacial waves (driven solely by gravity) on the transport process, and, second, to obtain conditions

which may prevail in the uppermost part of the packed-bed condenser reported by Bontozoglou and Karabelas [2], where, because of the significant condensation that has already taken place, the velocity of the gas phase is relatively small compared to the liquid film velocity.

For the thin liquid films treated here, it is usually assumed for convenience that, during condensation, the temperature profile in the liquid film is practically flat; e.g. Linehan *et al.* [15] and Segev *et al.* [16]. In the next section (Theory), three possible liquid temperature profiles (including the flat one) are assessed in a first attempt to model the complicated phenomena involved. The best model is selected and employed for interpreting the experimental data. The main experimental information involves accurate local temperature measurements along the tubular test section, leading to a determination of local condensation heat transfer rates. To get a more complete physical picture of the problem, parallel experiments were conducted to investigate the longitudinal variation of liquid film characteristics **under condensation,** and to compare them with similar data taken under isothermal conditions (Karapantsios and Karabelas [13]). This information is considered essential, providing insights into the mechanics of the process, in particular regarding the possible effect of condensation on the wave structure, as well as directly usable data for modeling. Finally, the data on wave characteristics are employed in an effort to correlate condensation heat transfer coefficients.

THEORY

Condensation in a multicomponent two-phase system causes variations in the amount and distribution of each phase [17]. These changes, in turn, induce variations in the local heat transfer processes. Because of the continuous change of all the thermal and hydraulic properties of the flow, the situation at any point along the transfer surface may never be truly fully developed either thermally or hydrodynamically. However, in order to describe the momentum and energy fields inside the two phases a pseudo-equilibrium state is customarily adopted in the literature.

Here, governing equations of our system are presented based on the following assumptions: the liquid film flow is steady and one-dimensional; steam is kept saturated throughout the pipe and gas pressure is constant; interfacial resistance is negligible, that is, the gas–liquid interface is at the saturation temperature, T_S, and the noncondensables are insoluble in the liquid. Free or forced convection in the vapour phase are not taken explicitly into account. However, the extent to which convection affects the transport process is a matter of concern, to be dealt with in a subsequent study.

The resistance to heat transfer on the gas side is considered first. Owing to accumulation of noncondensable gases near the interface, the condensing

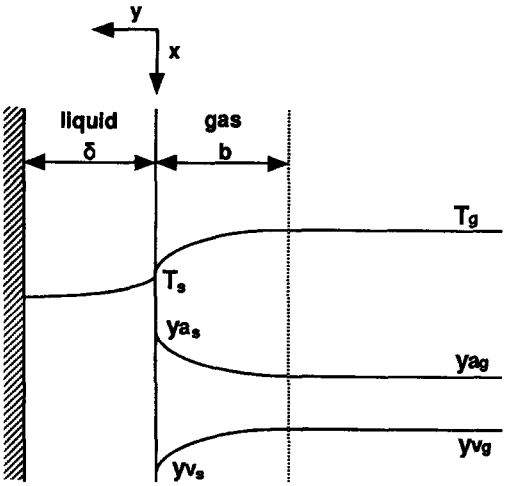

Fig. 1. Interface resistance to heat transfer due to the presence of noncondensable gases.

vapour must diffuse through a gas layer, which evidently acts as an additional resistance to heat transfer, as indicated in Fig. 1. Vapour diffusion gives rise to concentration and temperature gradients in the y-direction which are associated with a finite diffusive flux towards the interface. The heat transfer rate from the bulk gas mixture to the interface—at a point x along the pipe and for fixed total pressure, gas concentration and flow pattern—is given by (e.g. Collier [17])

$$q(T) = \frac{K_g \lambda \rho_g}{p_{am}} (p_{vg} - p_{vs}) + h_g (T_g - T_s) \qquad (1)$$

where $K_g = D_g/b$ and $h_g = k_g/b'$ are the mass and heat transfer coefficients, respectively,

It is impossible at present to describe in detail any possible *local* flow patterns that prevail on the gas phase due to free or forced convection (possibly induced by interfacial drag). Therefore, it seems appropriate to include all local flow field and transport effects in just a single phenomenological parameter. In fact, there are two such length parameters (b and b') in equation (1), introduced in the definitions of K_g and h_g. These are usually referred to as the *apparent mass and thermal boundary layers* at the gas side. In a previous analysis [14], it is shown that the second term on the right-hand side of equation (1), accounting for sensible heat transfer, has a relatively small contribution ($<10\%$) to the overall heat transfer rate even for vapours with large quantities of noncondensable gases (~ 0.90 air mole fraction). In this study, when the air mole fraction varies between 0.25 and 0.85, sensible heat transfer is considered negligible. Thus, one can use in the analysis a mass boundary layer equal to the thermal one ($b = b'$) without committing a significant error. To the knowledge of the present authors, a correlation for the apparent boundary layer thickness during condensation over a

vertical surface, with noncondensables present, is not available in the literature.

A first attempt to account for the liquid flow calls for the solution of an energy conservation equation by application of a velocity distribution, $u(y)$, and an effective thermal diffusivity function, $\alpha_e(y, T)$, henceforth referred to as the 'exact' solution. By neglecting wave effects it is further assumed that the liquid layer has a constant thickness, δ. The equation describing the thermal field inside a hydrodynamically developed liquid layer can be written as

$$u(y)\frac{\partial T}{\partial x} = \frac{\partial}{\partial y}\alpha_e(y, T)\frac{\partial T}{\partial y}. \tag{2}$$

The system of coordinates employed here is shown in Fig. 1. Boundary conditions representative of our system are:

$$x = 0, \quad T = T_i \tag{3}$$

$$y = 0, \quad -k\frac{dT}{dy} = q(T) \tag{4}$$

$$y = \delta, \quad -k\frac{dT}{dy} = 0. \tag{5}$$

Adiabatic conditions [equation (5)] are considered to represent this system well. A drawback of this formulation is that, at high flow rates (turbulent flow), the vanishing of the turbulent eddy diffusivity at the interface implies that the major resistance to heat transfer resides at the film surface. This is contrary to what is expected to occur in real systems where wave-induced turbulence near the free surface tends to enhance rather than reduce heat transfer.

The notion that the waves tend to minimize the temperature gradients normal to the flow lends support to the premise that the temperature across the entire liquid film may be practically uniform. In such a case, temperature varies only in the axial direction and the equation giving this dependence (henceforth referred to as the 'uniform' solution) is derived by integration of equation (2) with respect to y and division by δ, together with equations (4) and (5):

$$\frac{dT}{dx} = \frac{1}{U_{ave}\delta\rho c_p}q(T) \tag{6}$$

where $T \equiv T_{ave}$ (T_{ave} is the mass flow weighted average temperature across the film), and U_{ave} the average streamwise velocity, defined by

$$T_{ave} = \frac{\int_0^\delta Tu\,dy}{\int_0^\delta u\,dy} \quad \text{and} \quad U_{ave} = \frac{1}{\delta}\int_0^\delta u\,dy. \tag{7}$$

Details of the implementation of the above 'exact' and 'uniform' solutions are given by Karapantsios *et al.* [14]. The computational convenience associated with equation (6) is evident. The validity and significance of such a simplification were assessed in ref. [14], which compared results from the solution of equation (6) with results from equation (2) for very dilute steam–air mixtures (air mole fractions of 0.85 and 0.88), and proved to be satisfactory. It is noted that, with such a large amount of noncondensables as in the previous paper, the liquid side resistance to heat transfer is most likely negligible. However, in this investigation moderate noncondensable mole fractions are encountered (0.25–0.85) and therefore some resistance to heat transfer may also be offered by the liquid film.

Model development

A simple model including the effect of waves is presented next, also taking into account resistance to heat transfer on the liquid side. It is an intermediate between the two previous approaches as it combines a *wave region* of fully mixed liquid just at the interface, where the temperature is uniform due to wave activity, and a *substrate region*, adjacent to the wall, where resistance to heat transfer is exhibited. To separate the film thickness into two regions, the minimum film thickness, δ_{min}, of a time record is utilized. Thus, the wave region corresponds to a film thickness above δ_{min} while all values below δ_{min} are characterized as the substrate region. This quantity is considered to be more appropriate, especially for the higher flow rates, than the one reported by Dukler and his collaborators [18, 19] based on the modal thickness, as pointed out by Karapantsios *et al.* [11]. The liquid flow in the substrate region is assumed laminar for the range of liquid flow rates employed in the calculations (1.7–17.5 g s^{-1} cm^{-1}) as it accommodates only a small portion of the total liquid flow and moves with a relatively small velocity close to the wall. The range of δ_{min} is from 0.15 to 0.23 mm, respectively. For computational convenience, the same δ_{min} is assumed at all axial distances, taken as the average of the corresponding δ_{min} values measured at the six measuring stations along the condensing surface of the present experimental set-up. Yet, as Karapantsios and Karabelas [13] showed, δ_{min} is a very weak function of the axial distance.

The energy equation for the wave region is

$$\frac{dT_{wave}}{dx} = \frac{q(T)}{\Gamma_{wave}c_p} \tag{8}$$

where T_{wave} denotes the uniform temperature and Γ_{wave} the mass flow rate per unit width. Γ_{wave} is calculated from the total mass rate, Γ_{tot}, by subtracting the mass rate of the substrate, Γ_{sub}:

$$\Gamma_{wave} = \Gamma_{tot} - \Gamma_{sub} \tag{9}$$

where $\Gamma_{sub} = \rho g\delta_{min}^3/3\nu$, in the laminar substrate.

The energy equation for the substrate is

$$u_{sub}(y)\frac{\partial T_{sub}}{\partial x} = \frac{\partial}{\partial y}\left[\alpha(T_{sub})\frac{\partial T_{sub}}{\partial y}\right] \tag{10}$$

where T_{sub} denotes the temperature and $u_{sub}(y)$ the

velocity distribution in the substrate. In this model only, $y = 0$ corresponds to the interface position between the substrate and wave regions. $u_{sub}(y)$ is given by the parabolic profile

$$u_{sub}(y) = \frac{g\delta_{min}^2}{2\nu}\left[1-\left(\frac{y}{\delta_{min}}\right)^2\right] \tag{11}$$

and the molecular diffusivity, $\alpha(T_{sub})$, is approximated as a linear function of T_{sub}:

$$\alpha(T_{sub}) = c_1 + c_2 T_{sub}. \tag{12}$$

The representative boundary conditions are:

$$T_{wave}(x) = T_{sub}(x, y = 0) \tag{13}$$

$$\left(\frac{\partial T_{sub}}{\partial y}\right)_{y=\delta_{min}} = 0. \tag{14}$$

New dimensionless variables are defined next:

$$y' = 1-2\frac{y}{\delta_{min}} \qquad x' = \frac{x}{L}$$

$$\Theta = \left[T - T_i + \frac{c_2}{c_1}(T-T_i)^2\right]\Big/(100\,\mathrm{K})$$

where L is the variable axial distance between successive measuring stations. Equations (11) and (12) become, respectively:

$$u'_{sub}(y') = \frac{2\nu u_{sub}(y')}{g\delta_{min}^2} = 1-\frac{(1-y')^2}{4} \tag{15}$$

and

$$\alpha'(\Theta_{sub}) = \frac{2\nu L\alpha(\Theta_{sub})}{g\delta_{min}^4}$$

$$= \frac{\nu L}{g\delta_{min}^4}[2(c_1 + c_2 T_i) + c_1(-1+\sqrt{1+400\Theta_{sub}c_2/c_1})].$$

Upon carrying out the foregoing transformation of variables, the conservation equations are reduced from a convection–diffusion to a diffusion-alone problem; i.e.:

$$\frac{d\Theta_{wave}}{dx'} = \left[1+2\frac{c_2}{c_1}(T_{wave}-T_i)\right]\frac{Lq}{100c_p\Gamma_{wave}} \tag{16}$$

$$u'_{sub}(y')\frac{\partial\Theta_{sub}}{\partial x'} = \alpha'(\Theta_{sub})\frac{\partial^2\Theta_{sub}}{\partial y'^2}. \tag{17}$$

The appropriate boundary conditions to equations (16) and (17) are:

$$\Theta_{wave}(x' = 0) = 0 \tag{18}$$

$$\Theta_{sub}(0, y') = 0 \tag{19}$$

$$\Theta_{sub}(x', 1) = \Theta_{wave}(x') \tag{20}$$

$$\left(\frac{\partial\Theta_{sub}}{\partial y'}\right)_{y'=-1} = 0. \tag{21}$$

It must be noted here that, for the solution of the model equations, no explicit use of a specific mean film thickness, δ_{mean}, is made. Instead, mass flow conservation is applied for the wave region, so as to relax the assumption of a smooth film interface of constant thickness. Numerical techniques employed to solve model equations (15)–(21) are outlined in the Appendix.

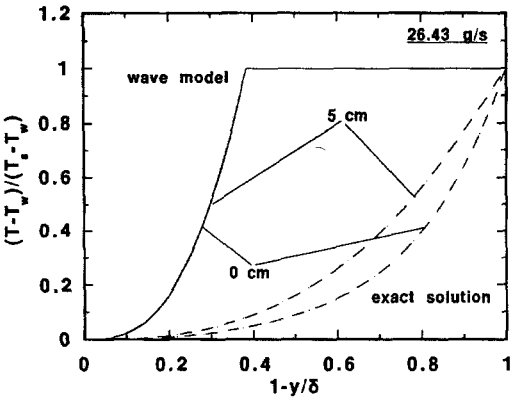

Fig. 2. Comparison of temperature profiles across the liquid film.

The cumulative condensation rate up to a distance x is calculated by the equation

$$\frac{d\dot{m}}{dx'} = \frac{D_g\rho_g L\pi D}{b}\log\left[\frac{1-x'_i(T_{wave})}{1-x'_i(T_g)}\right]. \tag{22}$$

The mass flow weighted average temperature, T_{ave}, is given by

$$T_{ave} = \frac{\Gamma_{sub}}{\Gamma_{tot}}\frac{3\pi}{4N}\sum_{i=1}^{N-1} T(\Theta_i)\sqrt{1-y_i'^2}\,u'_{sub}(y'_i)$$

$$+\frac{\Gamma_{wave}}{\Gamma_{tot}}T_{wave}. \tag{23}$$

In the forthcoming calculations, the variation of liquid properties within the flowing film is taken into account at each point of the computational domain while for the gas phase all physical properties are evaluated at the bulk temperature of the mixture. All property values are obtained from *VDI—Wärmeatlas* [20]. It appears that the reliability of computational results is appreciably affected by the proper choice of fluid properties, as also reported by Minkowycz and Sparrow [7].

Comparison of models

Sample calculations are performed at various inlet liquid flow rates. Solutions are obtained by matching the computed film wall temperatures with the experimentally determined ones at all six measuring stations of the present set-up. Results for a low initial liquid flow rate (26.43 g s^{-1}) are compared in Fig. 2. This low flow rate is chosen because, at these laminar flow conditions, a comprehensive examination of all models is more appropriate since the wave-induced turbulence and mixing activity are small. That is,

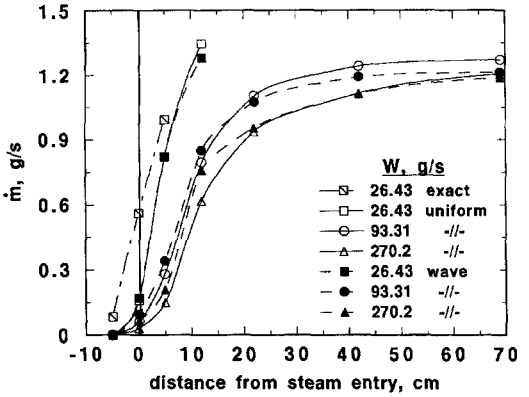

Fig. 3. Comparison of the cumulative condensation rates along the test tube predicted by the three theoretical models.

for higher flow rates (>43.7 g s^{-1}), after the onset of turbulence, the 'exact' solution gradually fails to predict the thermal field within the liquid since wave effects are totally ignored in this model.

Temperature profiles at only two locations along the test tube are given, at the level of the steam entrance (0 cm) and 5 cm further downstream (5 cm) i.e. over a distance where a significant part of the condensation is expected to take place. In the specific experimental set-up employed in this study (see next section) limited condensation takes place upstream of the steam entrance level. The uniform temperature solution, $T \equiv T_w \equiv T_s$, cannot be presented in Fig. 2 due to the scale factor chosen for the vertical axis. However, this solution is somewhat redundant inasmuch as it is represented by just a constant value. So, in order to assess the other two models, a scale factor, $T_s - T_w$, is selected to facilitate the presentation. As is shown in this graph, the two models give completely different T-profiles; but they both successfully predict a reasonable thermal field inside the liquid layer at these specific axial distances along the test-tube. Moreover, calculations for other longitudinal distances prove that the 'exact' model is incapable of describing the measured wall temperatures further downstream along the condensing surface by considering condensation alone.

Regarding the predicted cumulative condensation rates, $\dot{m}$, a comparison is offered in Fig. 3, for three flow rates: a low, a moderate and a high one. Predictions for the lower flow rate (26.43 g s^{-1}) are restricted to a 12 cm downstream distance. This is so—as will be explored in detail in a subsequent section—because at this distance the liquid attains an elevated surface temperature, equal or higher than the adjacent gas mixture saturation temperature, so that not only condensation stops but the reverse evaporation phenomena also start. Upon inspection of Fig. 3, the 'exact' solution appears substantially different from the other two, predicting much higher condensation rates. This is expected because thermal energy dissipation within the liquid by diffusion alone is quite a slow process, requiring large driving forces (condensation rates) to occur within a short distance. The 'exact' model appears to be deficient regarding physical descriptions such as hydrodynamic (no waves) and geometrical (smooth interface) details. In view of its inability to describe the thermal field at higher flow rates and longer distances, it will not be used in the rest of the calculations of this study. On the other hand, predictions from the 'uniform' and 'wave' models are very close. However, the 'wave' model appears in general superior to the 'uniform' solution. Indeed, at the higher flow rates where an almost flat temperature profile exists, the flow rate through the substrate region (<0.23 mm) is only a very small part of the total ($\sim 7\%$). Therefore, the 'wave' model is selected for the calculations and comparisons that follow. The mean deviation between the two models, with respect to the condensation rates over the whole range of liquid flow rates and gas mixture concentrations encountered in this study, is 20%, the maximum deviation being up to 70%.

APPARATUS AND EXPERIMENTS

A schematic of the loop is shown in Fig. 4. The experimental set-up and test procedure are described in detail elsewhere [21]. A vertical, transparent, Plexiglass pipe of 50 mm i.d. and 2.66 m total length is used, divided into three sections, i.e. inlet (0.3 m), intermediate (0.9 m) and measurement section (1.40 m). Sufficient external insulation is used to achieve adiabatic conditions. The vertical alignment of the entire tube-assembly is checked by a land-surveying precision instrument, a theodolite (maximum deviation from vertical $<0.01°$). Filtered, deaerated tap water (stored in a large tank) is used in the tests, flowing only once through the system. The water in the tank is at room temperature at all times. A continuous uniform feed inside the vertical tube is obtained by the liquid freely running over a tapered feeding entry. Flow rates from 26 to 416 g s^{-1} are employed.

Steam comes from the building supply at a pressure of 4 bar. It is passed through a conditioning set-up involving two separators, a steam trap and a pressure regulator which reduces the line pressure to only 1.5 atm so as to minimize the discharge velocity when entering the test pipe. This procedure provides a slightly superheated steam, relatively free of air ($<10^{-3}$ mass fraction air in mixture). Excess steam is discharged to the atmosphere through a vent located in the downstream receiving vessel.

Steam is released inside the pipe, at the center of the cross-section, in the direction of the liquid flow. A specially designed feeding section made of a perforated Teflon end-piece is used to spread the steam in the test-tube, and minimize the forced-convection effects. The system is allowed to operate with steam at a fixed liquid rate for almost an hour to reach a steady state. It is then observed that, upon discharge to the test section, steam is mixed with air, which

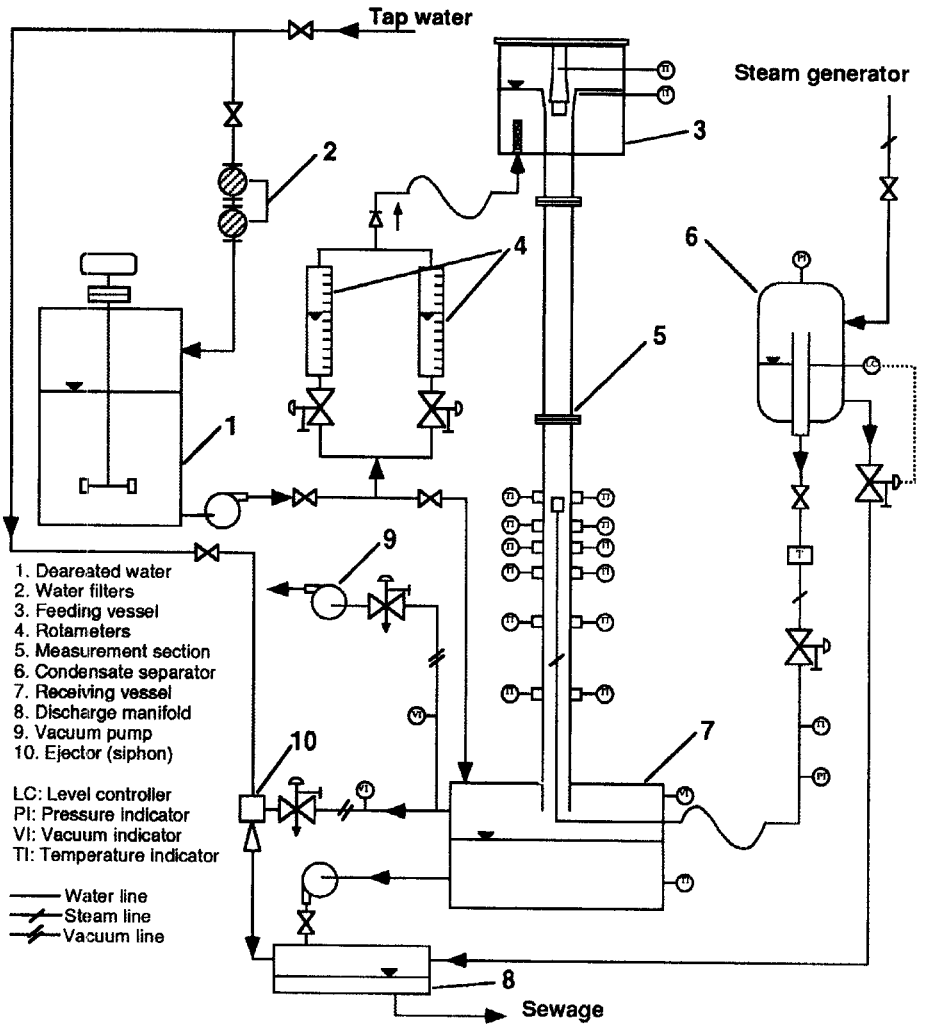

Fig. 4. Experimental set-up.

appears to move downwards from the upper part of the pipe, possibly dragged by the interfacial shear exerted by the fast moving liquid. As a result, the steam–air mixture apparently moves with a finite velocity which, however, is under all circumstances small enough (of order 10 cm s^{-1}), compared to the liquid film velocity (of order 1 m s^{-1}). Thus, the gas phase may be considered effectively stagnant. The steam entrance level is 1.77 m below the liquid feed. At that level the falling film flow is considered (e.g. Zabaras [19] and Takahama and Kato [22]) almost fully developed, facilitating the interpretation of local condensation measurements.

In addition to measuring inlet water flow rates and temperatures, and inlet steam conditions, the temperature of the liquid film and the steam–air mixture are measured at selected locations along the tube below the liquid feed level. For this reason, the test section is equipped with six pairs of (diametrically opposite) plugs mounted flush with the inner surface of the pipe. The plugs are aligned at the same azimuthal location at downstream distances of 1.72, 1.82, 1.89, 1.99, 2.19 and 2.46 m. Considering the steam entrance level (1.77 m) as the reference 'zero' point, the aforementioned distances are designated (and referred to in the rest of this study) as −5, 5, 12, 22, 42 and 69 cm, respectively.

A complete set of temperature measurements, to obtain liquid temperature time records, is conducted using copper–alumel thermocouples (T-type, 0.0127 cm dia. wire) embedded in the—oriented 180° apart—plugs, almost flush with the inner wall. The exact location of the tip of a thermocouple is a matter of concern. In preliminary tests, it was observed that a thermocouple bead partly projected into the liquid layer creates a wake that may alter the local flow field, and it is uncertain at what downstream distance this effect will vanish. Consequently, the downstream temperature measurements might be influenced by upstream conditions. Even with the thermocouple tip flush with the wall, some flow distortion may be caused due to the difficulty of constructing the ther-

mocouple bead to a curvature identical to the curvature of the test section. In view of these difficulties it was decided to measure the **outer** wall surface temperature by self-adhesive T-type (0.0127 cm dia.) thermocouples, mounted on the outer surface of the Plexiglass tube and then apply Fourier's law across the wall thickness to determine the **inner** wall surface temperature. These types of measurements are performed at exactly the same location as the plugs but 90° apart in the circumferential direction. All thermocouples are calibrated to 0.1°C. Comparison between measurements from thermocouples in contact with the liquid film and others mounted at the outer Plexiglass wall revealed that systematic slightly elevated temperatures are obtained from the former. In the subsequent sections of this work only the latter measurements will be presented.

The average gas mixture temperature is obtained by rigid-stem thermocouples protruding into the core of the pipe through appropriate gauges mounted on the plugs. The exact radial location of the most representative gas mixture temperature is a matter of concern. A large number of tests are performed (see next section) and transverse gas temperature profiles are determined at various flowrates and downstream locations. The nearest feasible position to the interfacial waves, without touching them even at the highest flow rates, is selected as the most suitable location to measure the gas bulk temperature. This is determined to be about 8 mm from the inner pipe wall.

The output from the self-adhesive thermocouples is sampled at 10 Hz for periods of 5–10 min. Exposed thermocouple measurements are sampled at 50 Hz for 100 s. The sampling interval is much smaller than the time constant of the thermocouples employed. Details of data collection and treatment are given elsewhere [21]. Repeatability checks are made for each set of conditions, giving very satisfactory results.

The parallel-wire electrical conductance probe is used in this work in order to measure local instantaneous fluctuations of the liquid film thickness. This technique is quite sensitive and accurate for this type of measurement; e.g. Karapantsios *et al.* [11]. Probes are fabricated for all six measuring stations along the test tube. Each probe consists of a pair of chromel parallel wires glued in a plug. The film thickness measurement is based upon a unique relationship between electrical resistance and depth of the wire immersion. Probe calibration is carried out outside the measurement tube-section. Calibration procedures and electrical signal conversion to film thickness are described in detail elsewhere [21]. Calibration is performed under isothermal conditions. It was hoped that, by applying a conductivity–temperature reference curve, it would be possible to convert the sampled voltage signals (during condensation) to the corresponding film thickness at the measured average temperature of the film cross-section. However, the wires, part of which extend into the steam–air mixture, are at an apparently higher temperature than the actual film temperature, causing a small conductivity reduction. Thus, an appreciable error is introduced into the measurement, and therefore film thickness records during condensation are only qualitatively considered in this work. However, frequencies and streamwise wave velocities, deduced from these signals, are still meaningful. To permit simultaneous film thickness measurements at different locations, each conductance probe is connected to a separate electronic analyzer. Testing and calibration of the analyzers' circuits is done prior to and after each set of experiments.

Thickness data are taken over a 10 s period with a 400 Hz sampling frequency. Exploratory runs with sampling frequencies 1, 5 and 10 kHz, at various liquid flow rates, did not alter the picture of the measured voltage traces. This indicates that, for the particular probe geometry, a 400 Hz sampling frequency provides an adequate temporal resolution, higher than typical maximum dominant frequencies of film records. Three records are acquired at each flow rate and at all locations to check for repeatability, and further increase the confidence of the calculated statistics. The estimated cumulative error in film thickness measurement—including calibration, measurement, digitization and data handling—is always less than 7%. The uncertainty in calculating the average wave velocity by the cross-correlation of two simultaneous film thickness records, sampled at different stations, depends on the particular probes' spacing at the given sampling resolution (400 Hz). Worst-case estimates of the calculated wave velocities are within 18% of the reported value.

RESULTS AND DISCUSSION

Liquid film characteristics

Figure 5(a) displays the average wave velocity, V_{wave}, plotted vs the longitudinal distance. The liquid flow rate is used as a parameter. This velocity is estimated by dividing the distance between two measuring stations by the time delay corresponding to the peak cross-correlation function of the respective thickness time records. As is well known (e.g. Takahama and Kato [22] and Karapantsios *et al.* [11]) this velocity is representative of the large roll waves which dominate at the falling film interface. The data of Fig. 5(a) correspond to experiments during condensation. An inspection of Fig. 5(a) reveals that the wave velocity tends to increase with increasing distance from the steam feed point. A somewhat peculiar behavior is noted for 26.43 and 31.36 g s^{-1}, not far below the steam entrance point; an appreciably lower velocity. As will be shown later, the region just below the steam distributor has a higher gas mixture temperature and therefore surface tension gradients are expected to be more pronounced there. However, to what extent such surface tension effects are responsible for the aforementioned peculiar behavior is unclear. Interestingly, data taken at this setup under isothermal conditions

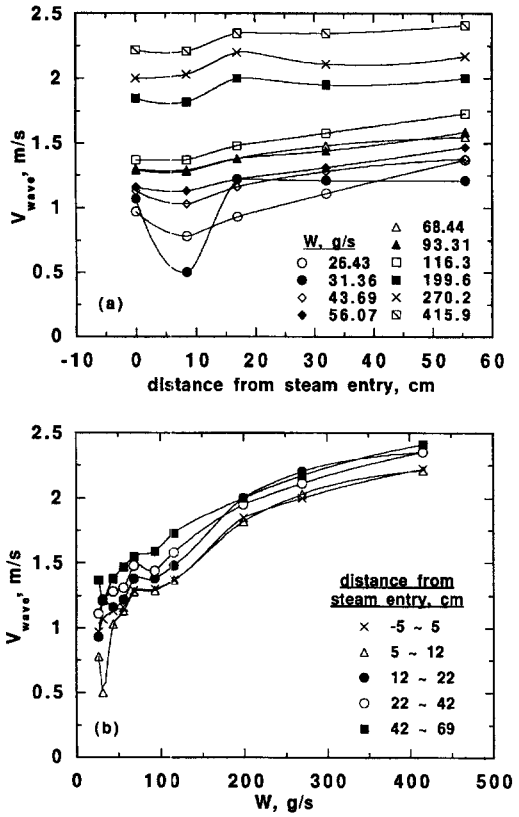

Fig. 5. Variation of the average wave velocity, V_{wave}, with: (a) longitudinal distance, (b) liquid flow rate.

[13] agree in general quite well with those of Fig. 5(a), especially if one takes into account the uncertainty in estimating wave velocities (up to 18%). The values and the trends reported by Zabaras [19] for isothermal films at similar axial distance (1.7–2.3 m) agree fairly well with the observations of this work.

As can be seen in Fig. 5(b) the wave velocity increases with increasing liquid flow rate. The increase is more rapid at low W. The same behavior is also noticed for velocities under isothermal conditions [21]. This observation probably reflects the fact that condensation is responsible only for relatively minor modifications of the isothermal film surface morphology. It appears that surface tension gradients and condensate formation may have an impact on ripples and small interfacial disturbances but not on larger lumps of liquid. It will be noted that Barry and Corradini [8], for condensation on a horizontal cocurrent flow of steam–air mixture over a subcooled liquid layer, observed reduced large wave amplitudes and wavelengths in comparison to those from isothermal experiments.

The power spectral density functions of the film thickness time records, both under isothermal conditions and during condensation, are computed from the probe signals with a method recently employed by Karapantsios *et al.* [11]. Spectra for all conditions are calculated. No discernible dependence on downstream distance is observed in all cases, indicating that at the axial locations examined in this study the wave energy distribution remains essentially the same. This is in accord with observations by Takahama and Kato [24] for distances greater than 1.3 m. All spectra from condensation experiments exhibit peaks close to those of the isothermal case but fall off more gradually in both directions; i.e. they are broader. For example, for $W = 26.43$ g s^{-1}, while the isothermal spectrum shows a dominant frequency around 6 Hz, the corresponding condensation spectrum displays a dominant frequency band between ~4 and 9 Hz. For $W = 270.2$ g s^{-1}, the isothermal spectrum peaks at ~8 Hz while the condensation signal is in the range ~3 to ~12 Hz. A broader peak than the usual isothermal case is also reported by Barry and Corradini [8] for direct contact condensation of steam–air mixtures flowing over a horizontal stratified water layer.

Temperature measurements

One major issue raised in the preceding section (Apparatus and Experiments), is the selection of the cross-sectional location inside the tube, where the steam–air mixture conditions best represent the bulk gas conditions. For this reason numerous preliminary experiments were conducted to investigate the transverse gas temperature profiles in the pipe at different downstream locations and liquid flow rates. Figure 6(a)–(c) displays the observed temperature profiles at three different flow rates. The dashed line indicates the maximum film thickness averaged over all measuring stations under isothermal conditions. Data points right on the ordinate axis represent inner wall surface temperatures. It is easily recognized that, for locations up to 12 cm below steam entry, the cross-sectional profiles are approximately flat outside the liquid region. For locations further downstream (>22 cm), where the gas phase is depleted of steam, a nearly parabolic profile prevails. It is noted that during these preliminary tests the steam entrance conditions were somewhat different than during the main course of the experiments; the steam line pressure just before discharge into the (1 atm) test tube was 1.2 atm instead of 1.5 atm as reported in the rest of this study. This difference is responsible for slightly different temperatures in the gas mixture but qualitatively the trends observed in Fig. 6(a)–(c) are expected to hold. After data assessment, it was decided that the most reliable gas bulk conditions are those obtained as close to the interface as possible, but without intersecting the interfacial waves. By estimating that the gas boundary layer thickness under the conditions of this study is of the order of few millimeters (< ~4 mm) [7], 8–9 mm away from the inner pipe wall is considered a reasonably good location to measure the representative gas bulk temperatures, T_g.

The time-averaged gas bulk temperature, T_g, is plotted against the longitudinal distance [Fig. 7(a)] and the liquid flow rate [Fig. 7(b). The highest temperatures are observed near the steam feed level. It is

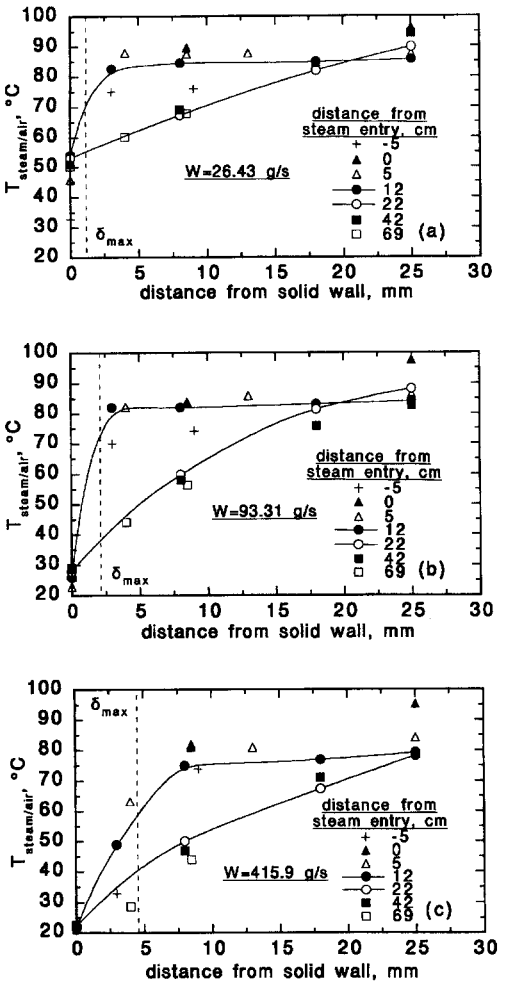

Fig. 6. Steam–air temperature profiles across the test tube at three different liquid flow rates: (a) $W = 26.43$ g s^{-1}, (b) $W = 93.31$ g s^{-1}, (c) $W = 415.9$ g s^{-1}.

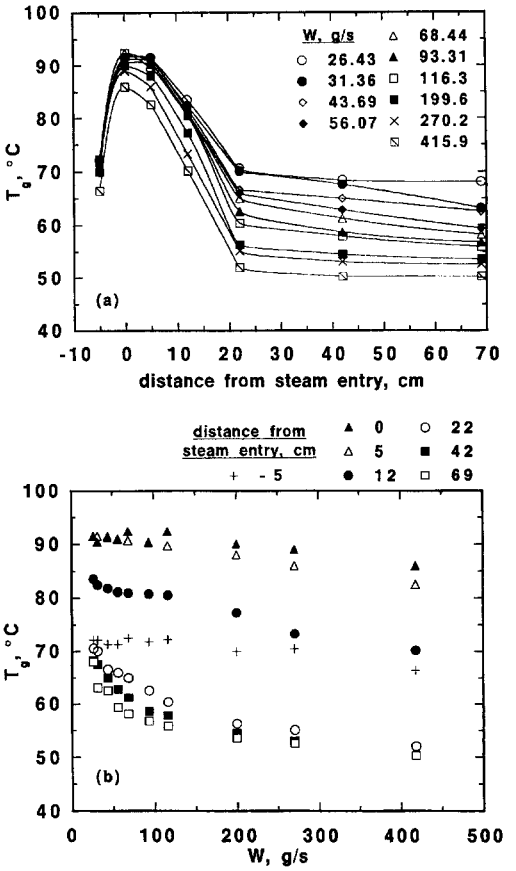

Fig. 7. Variation of T_g with: (a) longitudinal distance, (b) liquid flow rate.

noted that some steam escapes upwards through the narrow gap between the liquid layer and the Teflon steam distributor. For axial distances of less than 22 cm [Fig. 7(a)] the gas mixture temperature falls off rather sharply, while for distances greater than 22 cm only gradually. It will be recalled that these temperatures correspond to saturation conditions so that steam mole fractions can be directly determined from these data. The respective steam mole fractions vary between ~ 0.15 and ~ 0.75. The variation of T_g with liquid flow rate [Fig. 7(b)] greatly depends on location. For locations down to 12 cm from steam feed and, for $W < 100$ g s^{-1}, T_g is fairly constant while, for $W > 100$ g s^{-1}, it gradually drops. For locations below 22 cm, the data exhibit a different behavior, showing a steeper decline with increasing W.

Attention is directed next to the temperatures measured at the inner pipe wall. This information is shown in Fig. 8(a) and (b). With respect to the longitudinal distance [Fig. 8(a)], T_w increases at all but the three lowest flow rates. For these particular flow rates, the inlet film temperature is initially raised for a distance 12 cm below the steam entry, due to steam condensation. After this point a temperature drop is observed, probably associated with evaporation. This is possible because for such low flow rates the hot interface may attain a temperature above the saturation temperature corresponding to the interfacial noncondensables concentration. Obviously, the interface is richer in noncondensables than the gas bulk mixture [Fig. 7(a)]. Such a behavior is displayed by the top three curves of Fig. 8(a). For the rest of the flow rates the liquid surface temperature never reaches the saturation temperature and only condensation occurs along the entire test section. Figure 8(b) shows the variation of T_w with liquid flow rate. A sharp drop with W is noticed at almost all locations. It is noteworthy that for W greater than about 200 g s^{-1} the slope of the curves becomes very small, indicating that in this region T_w is weakly dependent on the flow rate.

Heat transfer coefficients

Consideration will now be given to the condensation heat transfer coefficient, h. It is defined as

$$h = \frac{\lambda}{\Delta T}\frac{\Delta W_c}{\Delta x} \tag{24}$$

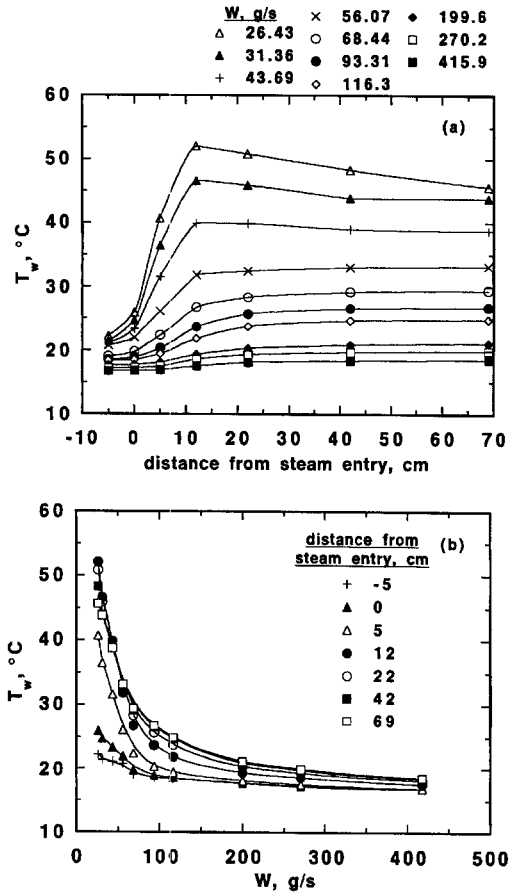

Fig. 8. Variation of T_w with: (a) longitudinal distance, (b) liquid flow rate.

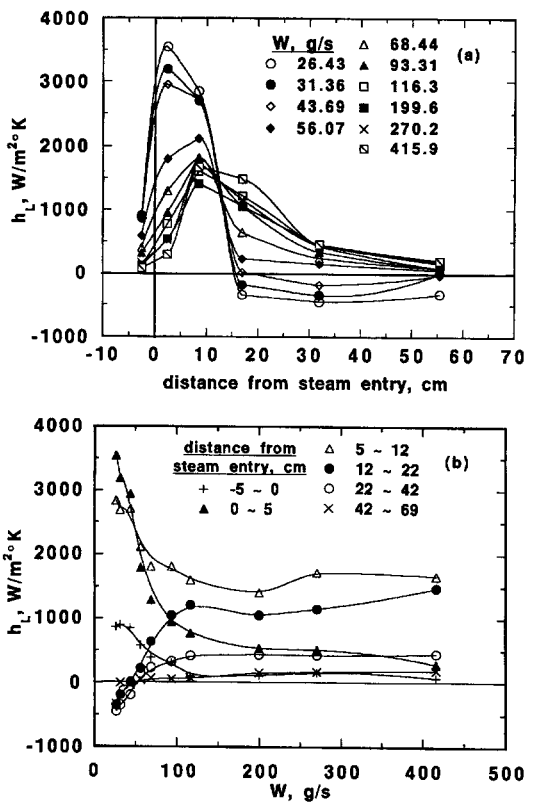

Fig. 9. Local condensation heat transfer coefficient, h_L, vs: (a) longitudinal distance, (b) liquid flow rate.

where $\Delta x = x_i - x_{i-1}$ is the distance between measuring stations i and $(i-1)$ to which h corresponds, ΔW_c is the condensation rate in g s^{-1} cm^{-1} and ΔT is the thermal driving force. For the local heat transfer coefficient h_L, ΔT is expressed as the difference $(T_g - T_{cm})$, where $T_g = (T_{gi} + T_{gi-1})/2$ and $T_{cm} = (T_{cmi} + T_{cmi-1})/2$. For the cumulative heat transfer coefficient, h_{CUM}, calculated from the steam entrance level down to a specific measuring position, the corresponding logarithmic mean temperature difference ΔT_{ln}, is employed. This ΔT_{ln} is determined by integration along the entire length in question, assuming h_{CUM} to be constant throughout. ΔT_{ln} is given as the ratio

$$(T_{cmi} - T_{cmi-1}) / \ln\left(\frac{T_{gi-1} - T_{cmi-1}}{T_{gi} - T_{cmi}}\right).$$

The mean error in calculating h_L and h_{CUM} is estimated to be less than 15%. For $h < \sim 300$ W m^{-2} K^{-1}, the error may be up to 70% because small temperature differences (involving relatively larger errors) are encountered in the calculations. However, such low h are of limited importance.

In Fig. 9(a) and (b) local heat transfer coefficients, h_L, computed from the data by employing the wave-model equations, are plotted vs the longitudinal distance and inlet liquid flow rate, respectively. A comparison of Fig. 9(a) and (b) with Fig. 7(a) and (b) reveals that the higher coefficients are calculated in the regions of gas mixtures rich in steam. In general the presence of noncondensable gases has a tremendous influence in reducing condensation heat transfer. Negative heat transfer coefficients, indicative of evaporation, are also presented in Fig. 9(a) and (b). They are estimated from simple energy conservation balances without solving the model equations, and are included in the plot only to get a more complete physical picture. Upon inspection of Fig. 9(a), one observes that condensation heat transfer coefficients for $W < \sim 44$ g s^{-1} peak very near the steam feed location while for $W > \sim 55$ g s^{-1} the peak is shifted a bit further downstream. In all cases, some condensation takes place just upstream of the steam entry point for which the coefficients are also plotted. Some interesting and unexpected trends are observed in Fig. 9(b). For distances less than 12 cm from the steam entrance, the local coefficients appear to decrease first and gradually level off to a constant value with increasing liquid flow rate. On the other hand, for distances greater than 12 cm from the stream entrance, the coefficients first increase and then level off with increasing W. A similar inversion of the observed trends with increasing axial distance is also noticed in data by Bontozoglou and Karabelas [2]—their Fig.

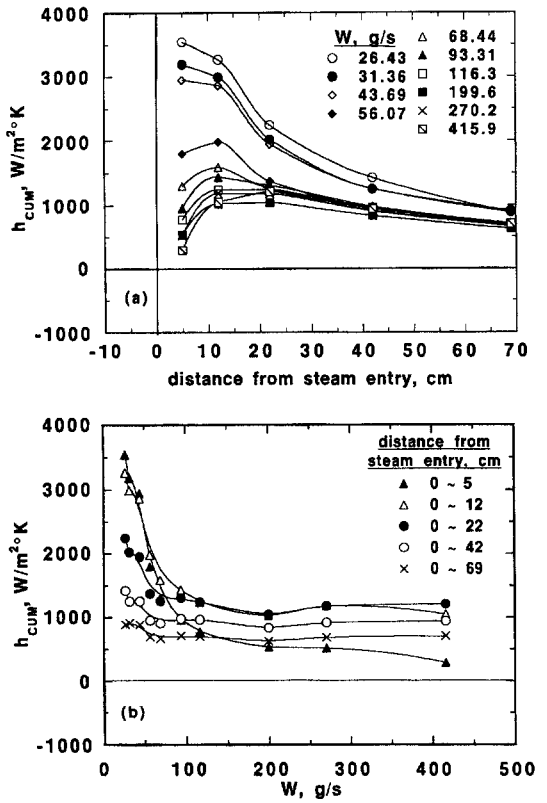

Fig. 10. Cumulative condensation heat transfer coefficient, h_{CUM}, vs: (a) longitudinal distance, (b) liquid flow rate.

4—from a direct-contact condenser with structured packing. Such changes apparently cannot occur in cases of condensation of steam, where condensation coefficients are expected to increase monotonically with increasing liquid flow rate.

The cumulative condensation heat transfer coefficient, h_{CUM}, is plotted against the longitudinal distance in Fig. 10(a) and against the inlet liquid flow rate in Fig. 10(b). It is obvious that integration over larger distances leads to lower coefficient values since the gas–vapour mixture becomes gradually depleted of steam. Interestingly, for the integration along the entire condensing surface (0–69 cm), all cumulative coefficients are within a narrow range ($\sim$500 to $\sim$1000 W m^{-2} K^{-1}). Furthermore, the evaporation occurring locally at the lower flow rates and at downstream locations $>$12 cm now vanishes by virtue of the overall averaging. Particularly, in Fig. 10(b) a monotonic decreasing trend with increasing W is observed. This is in line with observations reported by Karapantsios *et al.* [14] regarding integral-type data obtained in the same apparatus. However, no comparison can be made with the data of that work because a longer condensing surface (2.46 m) and more dilute steam–air mixtures were employed (air mole fractions of 0.85 and 0.88). The behavior demonstrated in Fig. 10(b) and, in part, in Fig. 9(b) is difficult to explain at present. An interpretation of this trend may be obtained by considering the large amount of noncondensables and the complex flow pattern that may develop in the gas phase by the interplay between the moving liquid interface and the adjacent gas layer. Such considerations are of no particular significance when just steam is condensed on subcooled liquid. It is likely that the effective gas boundary layer, b, greatly influenced by the gas flow distribution, is responsible for this behavior of the condensation rates. This point is further explored in a subsequent section.

As regards **direct-contact** experiments with noncondensables, the literature is indeed rather poor. To the best of the authors knowledge, there are only three systematic experimental investigations on the condensation of steam–air mixtures over subcooled liquid layers (Sadek [23], Chan and Yuen [9] and Barry and Corradini [8]). All three studies deal with direct-contact condensation over **horizontal** water layers where the free surface air-blanketing effect is strongly evident. Sadek [23] employed a nearly stagnant steam–air mixture with 0 to $\sim$7% air mass fraction and measured an overall coefficient, over a 3 ft long surface, varying between $\sim$11 000 and $\sim$500 W m^{-2} K^{-1}. Chan and Yuen [9] did local measurements with steam–air flowing cocurrently with a water layer for air mass fractions of 0–3.3%. The calculated coefficients varied between $\sim$12 000 and $\sim$800 W m^{-2} K^{-1}, respectively. The only investigation which employed higher air–steam mass ratios ($\sim$50 to $\sim$94%) was the work by Barry and Corradini [8]. Turbulence and waviness of the liquid layers were present in their tests. They reported overall heat transfer coefficients along a 1.83 m condensing surface of about 200–600 W m^{-2} K^{-1}. An important feature in their set-up, differing from ours, was the intensive forced convection on the gas side (gas velocities of 5.5 and 6.5 m s^{-1}). Although a comparison can be made only with reservations, it is noted that the data from this work [e.g. Fig. 10(a) and (b)] are in the same range of values as the results from the above studies.

Influence of waves on condensation rates

Attention is now directed to the possibility that the statistical characteristics of the wavy falling film may have some bearing on the size of the apparent gas boundary layer for mass transfer, b, defined in equation (1). By considering overall (integral) type data, Karapantsios *et al.* [14] observed a surprising similarity of the variation of the gas boundary layer, b, and of twice the standard deviation, $2s$, of liquid film thickness fluctuations. It was suggested that the quantity $2s$ might be quite representative of wave effects on the gas side resistance to heat transfer. This also seems to be in line with recent calculations by Karapantsios and Karabelas [12] on the Eulerian accelerations and decelerations of the liquid interface normal to the flow direction. However, the extent to which a possible relationship between b and s exists *locally* is inves-

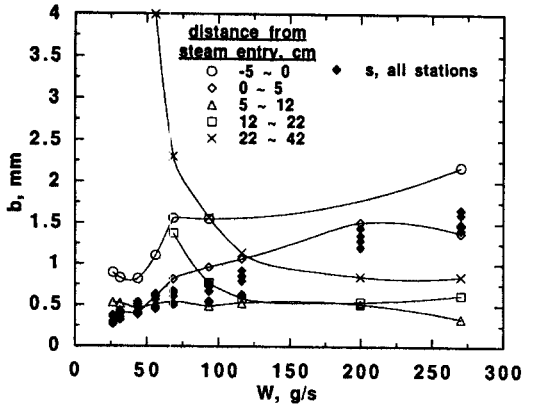

Fig. 11. Experimentally determined apparent boundary layer of noncondensables, b, and comparison with present statistical information of film thickness fluctuations.

tigated next. Figure 11 displays a comparison between the variation of the local gas boundary layer and the standard deviation of the corresponding local adjacent liquid film. The diffusion layer **does not** exhibit the same systematic trend for all longitudinal distances, but from initially increasing with W (-5 cm $< x <$ 5 cm), it levels off at a roughly constant value (5 cm $< x <$ 12 cm) and finally tends to decrease ($x >$ 12 cm) as W increases. This trend could have been expected in view of the nature of the gradually heated water layer which is thermally developing with distance. Comments similar to those presented in relation to Figs. 9(b) and 10(b) (on the possible interaction of the wavy liquid film with the neighboring gas layer) may also be made for interpreting the variation of the apparent boundary layer thickness, b. The literature is not helpful in this case since no revelant data for condensation are available. Finally, this behavior does not allow the development of a generalized equation to describe local b as a function of local s applicable to all locations. The relationship obtained by Karapantsios *et al.* [14] regarding overall condensation coefficients may still be useful for design purposes.

The gas boundary layer may be correctly estimated from the experimental data once the physical quantities that properly describe the transport process, from both the gas and the liquid phase, are included in the correlation. The ratio of the effective mass transfer film thickness to the momentum layer is described by a single parameter, the gas Schmidt number, Sc, which accounts for the diffusion flux alone. To account for possible free convection, the gas Grashof number, Gr, is introduced. As Karapantsios *et al.* [14] report for dilute steam–air mixtures, diffusion and free convection on the **gas** phase alone cannot account for the experimentally observed increase of the diffusion layer, b, with the **liquid** flow rate. It seems that forced convection, possibly induced by the flowing liquid layer, must be included to fully account for such a behavior. Thus, correlations proposed in the literature for the prediction of b, based solely on gas phase conditions (e.g. Akers *et al.* [24]) may not describe adequately phenomena that take place during condensation in systems like the present one. For such forced convection effects (i.e. induced by interfacial drag), liquid side and interfacial parameters may come into play. The most universal liquid parameter which may be included in such a gas mass transfer correlation (e.g. Fair and Bravo [3]) is the liquid Reynolds number, Re. Interfacial effects may be represented by well-known dimensionless groups, i.e. the Weber number, We, the Bond number, Bo, or the Capillary number, Ca.

As pointed out earlier, the interface is dominated by large, fast moving roll waves. To what extend these are influenced by interfacial effects (due to condensation) is difficult to ascertain. Indirect evidence obtained here, by measuring wave characteristics (velocity, frequency), suggests that such effects may not be important and that the roll waves are essentially unaffected. Additionally, typical values of the above dimensionless numbers, based on our data, are much greater than 10^3, suggesting that surface tension forces are insignificant in this case. Thus, the influence of We, Bo and Ca is not considered to be important.

Interfacial effects may be also accounted for explicitly by employing measured characteristics of the interface. A common definition of surface roughness is given as the ratio s/D, where s is the standard deviation of the film thickness fluctuations and D is the tube diameter. More important may be two new quantities which were proposed recently by Karapantsios and Karabelas [12] to describe dynamic interfacial film characteristics. They are the first and second time derivatives, of the continuous and discretized film thickness time record, $\delta(t)$, defined in a Eulerian frame of reference. By calculating the rate of surface displacement, $\mathrm{d}\delta/\mathrm{d}t$, of a film thickness time record and then taking its mean absolute value, a new quantity is determined, $|\mathrm{d}\delta|\mathrm{d}t|_{\mathrm{mean}}$, which represents the relative mean rate of surface displacement. Further division of this quantity by the average wave velocity estimated from the cross-correlation function, $V_{\mathrm{wave}} = \mathrm{d}x/\mathrm{d}t$, provides another measure of the average surface roughness, $\delta/x = |(\mathrm{d}\delta/\mathrm{d}t)|_{\mathrm{mean}}/(\mathrm{d}x/\mathrm{d}t)$. As shown elsewhere [13], $|\mathrm{d}\delta|\,\mathrm{d}t|_{\mathrm{mean}}$ ranges between ~ 10 and ~ 75 mm s^{-1} while V_{wave} [e.g. Fig. 4(a) and (b)] between ~ 0.5 and ~ 2.3 m s^{-1} for the liquid flow rates employed in this study.

Karapantsios and Karabelas [12] argue that the second time derivative, $\mathrm{d}^2\delta/\mathrm{d}t^2$, of the film thickness record is not only related to the local radius of curvature, R, of the liquid surface through the equation

$$\frac{1}{R} = \frac{\mathrm{d}^2\delta}{\mathrm{d}x^2} = \frac{1}{V_{\mathrm{wave}}^2}\frac{\mathrm{d}^2\delta}{\mathrm{d}t^2} \tag{25}$$

but also serves as an indicator of the inertial (energy dissipation) phenomena that accompany the surface undulatory motion. By taking the mean absolute

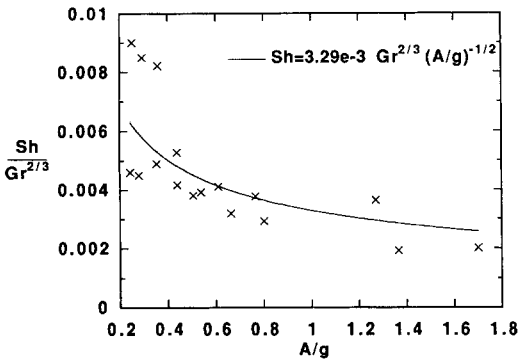

Fig. 12. Correlation of Sh for $Gr = 1.5$–4.5×10^6 and $A/g = 0.24$–1.7 ($Re = 900$–6500).

value of $d^2\delta/dt^2$, another quantity is defined, $|d^2\delta/dt^2|_{mean} \equiv A$. The values of R range between ~ 20 and ~ 50 cm and of A between ~ 2.5 and ~ 25 m s^{-2} for the liquid flow rates employed here [13, 23]. Thus, a new dimensionless parameter is introduced to account for both local geometry and inertia effects, A/g, where g is the gravitational acceleration.

To develop a correlation of the condensation rates measured here, expressed as the gas Sherwood number (Sh), the following dimensionless numbers could be used: Sc, Gr, Re, s/D, δ/x and A/g. A stepwise Graham–Schmidt decomposition scheme is employed to determine the best correlation among the various parameters. By considering data obtained at **all** locations along the condensing surface, a poor correlation is found among combination of variables, giving significant average errors ($> 60\%$). This could have been expected in view of the nature of the heated water layer which is thermally developing with axial distance. It was decided, therefore, to limit the correlation to similar conditions, i.e. those of neighboring regions. In view of its practical importance, the region within 12 cm downstream from the steam entrance level (0.46 < steam mole fraction < 0.74) is considered. The average Sh is best correlated as a function of Gr and the dimensionless acceleration A/g, as shown in Fig. 12:

$$Sh = 3.29 \times 10^{-3} Gr^{2/3} (A/g)^{-1/2}. \quad (26)$$

This correlation has a mean standard error of 0.09 and an average error of 21% significant at a 95% level. As indicated in Fig. 12 there is a good correlation for $0.4 < A/g < 1.7$. More data are needed to explore the discrepancy for $A/g < 0.4$. For practical applications the ratio A/g must be calculated from film thickness information. In this study, local A/g values correspond to local Reynolds numbers in the range $\sim 900 < Re < \sim 6500$. Moreover, A/g is correlated with Re by

$$A/g = 4 \times 10^{-3} + 2.6 \times 10^{-4} Re \quad (27)$$

which is considered reasonably accurate for practical calculations (mean error $\sim 10\%$). Upon inspection of equations (26) and (27), one observes that best predictions are obtained for $Re > \sim 1500$ (turbulent regime) since in this region A/g is greater than 0.4.

CONCLUSIONS

The present study provides new theoretical and experimental information regarding the local condensation rates of quasi-stagnant steam–air mixtures in direct contact with free falling wavy–turbulent water layers. The gas phase may be regarded as effectively stagnant insofar as its bulk velocity is small relative to the liquid surface velocity. This study is an extension of previous work (Karapantsios *et al.* [14]) which dealt with integral-type measurements in the same experimental set-up. Both studies are motivated by a parallel project, also in progress in this laboratory [2], for the evaluation of the performance of a direct-contact vertical condenser.

An assessment of three different theoretical models is made. For the air concentrations and liquid flow rates employed in this study a new 'wave' model is proposed which considers a resistance to heat transfer presented from both the gas and the liquid phase. An essential feature of this model is that it decomposes the liquid film into a wavy region, where a uniform temperature due to wave activity prevails, and a substrate region where some resistance to heat transfer exists. In order to relax the assumption of a smooth film surface of constant longitudinal thickness, the model does not make explicit use of the mean film thickness but rather of the minimum film thickness, which is less sensitive to longitudinal changes and only mass flow conservation is applied for the wave region. This model is employed to obtain heat transfer coefficients from the measured temperatures.

It is suggested that knowledge of the interface morphology during condensation is an essential prerequisite for the development of realistic condensation models incorporating wave characteristics. Experimental evidence on the average wave velocity and dominant frequency range of the liquid layers employed in this study reveals that the interface is only slightly modified by condensation. It seems that large roll waves remain practically unaffected and only small-amplitude surface disturbances are significantly damped.

The experimentally determined local condensation heat transfer coefficients, h_L, are greatly dependent on the local noncondensables concentration. They also display a rather unexpected behavior; with increasing liquid flow rate, h_L either increases or decreases depending on downstream measurement location. A similar behavior is also noted in the above-mentioned direct-contact condensation column [2]. This interesting trend is attributed to the complex flow patterns that may prevail at the interface on the gas mixture side as a result of the dynamic interplay between undulations of the liquid film and the adjacent gas layer.

The incapability to describe the experimentally observed increase of the apparent gas boundary layer,

b, with the liquid flow rate, in terms of gas phase conditions only, lends support to the use of a forced convection factor to account for this effect. Inasmuch as the gas phase is considered quasi-stagnant, the only additional convective motion may be induced by the wavy liquid surface. This is in line with a recent work by Karapantsios and Karabelas [12], who report that some complex momentum interchange may take place between the wave motion and the compressible gas phase, possibly inducing small-scale local flow at the gas side. To implement these results, a correlation for the local gas boundary layer, b (nondimensionalized as Sh), is proposed as a function of Gr and the dimensionless parameter A/g which characterizes the interface.

Acknowledgements—This work has been supported in part by the General Secretariat for Research and Technology of Greece and by the Commission of European Communities (under programme VALOREN and contract JOU2-CT92-0067). Helpful discussions with Dr V. Bontozoglou are greatly appreciated.

REFERENCES

1. F. Kreith and R. F. Boehm (Editors), *Direct-contact Heat Transfer*. Hemisphere, New York (1988).
2. V. Bontozoglou and A. J. Karabelas, Simultaneous direct-contact condensation and noncondensable gas absorption in columns with structured packing, *A.I.Ch.E. Jl* (in press).
3. J. R. Fair and J. L. Bravo, Distillation columns containing structured packing, *Chem. Engng Prog.* **86**(1), 19–29 (1990).
4. H. R. Jacobs, Condensation on immiscible falling films, ASME paper No. 80-HT-110, Orlando, FL (July 1980).
5. H. J. Kim, S. C. Lee and S. G. Bankoff, Heat transfer and interfacial drag in countercurrent steam–water stratified flow, *Int. J. Multiphase Flow* **11**, 593–606 (1985).
6. G. P. Celata, M. Cumo, F. D'Annibale, G. E. Farello and G. Focardi, A theoretical and experimental study of direct-contact condensation on water in turbulent flow, *Exp. Heat Transfer* **2**, 129–148 (1989).
7. W. J. Minkowycz and E. M. Sparrow, Condensation heat transfer in the presence of noncondensables, interfacial resistance, superheating, variable properties and diffusion, *Int. J. Heat Mass Transfer* **9**, 1125–1144 (1966).
8. J. J. Barry and M. L. Corradini, Film condensation in the presence of interfacial waves, *ASME Proceedings of the* 1988 *National Heat Transfer Conference*, Houston, TX, pp. 523–529 (1988).
9. T. S. Chan and M. C. Yuen, The effect of air on condensation of stratified horizontal cocurrent steam/water flow, *ASME J. Heat Transfer* **112**, 1092–1095 (1990).
10. D. Hasson, D. Luss and U. Navon, An experimental study of steam condensation on a laminar water sheet, *Int. J. Heat Mass Transfer* **7**, 983–1001 (1964).
11. T. D. Karapantsios, S. V. Paras and A. J. Karabelas, Statistical characteristics of free falling films at high Reynolds numbers, *Int. J. Multiphase Flow* **15**, 1–21 (1989).
12. T. D. Karapantsios and A. J. Karabelas, Surface characteristics of roll waves on free falling films, *Int. J. Multiphase Flow* **16**, 835–852 (1990).
13. T. D. Karapantsios and A. J. Karabelas, Longitudinal characteristics of wavy falling films, *Int. J. Multiphase Flow* **21**, 119–127 (1995).
14. T. D. Karapantsios, M. Kostoglou and A. J. Karabelas, Direct contact condensation of steam on wavy falling films, Paper D4, 29th Meeting of the European Two-Phase Flow Group, Stockholm, 1–3 June (1992).
15. J. H. Linehan, M. Petrick and M. M. El-Wakil, The condensation of a saturated vapour on a subcooled film during stratified flow, *A.I.Ch.E. Prog. Symp. Ser.* **66**(102), 11–20 (1970).
16. A. Segev, L. J. Flanigan, R. E. Kurth and R. P. Collier, Experimental study of countercurrent steam condensation, *ASME J. Heat Transfer* **103**, 307–311 (1981).
17. J. G. Collier, *Convective Boiling and Condensation*. McGraw-Hill, London (1972).
18. K. J. Chu and A. E. Dukler, Statistical characteristics of thin, wavy films, Part II. Studies of the substrate and its wave structure, *A.I.Ch.E. Jl* **20**, 695–706 (1974).
19. G. J. Zabaras, Studies of vertical annular gas–liquid flows, Ph.D. Thesis, University of Houston (1985).
20. *VDI—Wärmeatlas, Berechnungsblätter für den Wärmeübergang*, 2. Auflage. VDI–Verlag GmbH, Dusseldorf (1974).
21. T. D. Karapantsios, Flow of a thin liquid film in a vertical pipe. Direct-contact condensation phenomena, Doctoral Dissertation (in Greek), Department of Chemical Engineering, University of Thessaloniki (1994).
22. H. Takahama and S. Kato, Longitudinal flow characteristics of vertically falling liquid films without concurrent gas flow, *Int. J. Multiphase Flow* **6**, 203–215 (1980).
23. S. E. Sadek, Condensation of steam in the presence of air, *Ind. Engng Chem. Fundam.* **7**, 321–324 (1968).
24. W. W. Akers, S. S. Davis and J. E. Crawford, Condensation of a vapor in the presence of a non-condensing gas, *Chem. Engng Prog. Symp. Ser.* **56**, 139–144 (1960).
25. J. Villadsen and M. L. Michelsen, *Solution of Differential Equation Models by Polynomial Approximation*. Prentice-Hall, Englewood Cliffs, NJ (1978).
26. C. Canuto, M. Y. Hussaini, A. Quarteroni and T. A. Zang, *Spectral Methods in Fluid Dynamics*, p. 69. Springer-Verlag, New York (1988).

APPENDIX: NUMERICAL SOLUTION OF THE 'WAVE' MODEL

The best method to solve equations (15)–(21), henceforth to be referred to as the 'wave' solution, is orthogonal collocation. A Chebyshev–Lobatto collocation [26] is preferred because the task is to match the computed temperature of the wall with the experimentally measured one. This collocation algorithm distributes the collocation points at the boundaries of the integration domain, giving higher precision over these regions. Moreover, the collocation points and the derivatives of the Lagrange polynomials at these points are given explicitly. In carrying out the solution, $N+1$ collocation points are used, y_i' $(i = 0, \ldots, N)$. Right at the boundary between the two regions, i becomes 0, (y_0'), and the substrate temperature equals that of the wave region. In addition to the equation for Θ_{wave}, equation (16), the following differential equations must be solved at the collocation points k:

$$\frac{d\Theta_k}{dx'} = \frac{\alpha'(\Theta_k)}{u'_{sub}(y_k')}\left(\sum_{i=1}^{N-1} C_{ki}\Theta_i + C_{k0}\Theta_{wave}\right) \qquad (A1)$$

where

$$C_{ki} = A_{ki} - \frac{A_{kN}D_{Ni}}{D_{NN}}$$

and

$$A_{ki} = \sum_{j=0}^{N} D_{kj}D_{ji}, \quad k = 1, \ldots, N-1. \qquad (A2)$$

D_{ij} are the elements of the differentiation matrix of the

Chebyshev–Lobatto collocation method given by Canuto *et al.* [26]. The value of Θ at the wall is given as

$$\Theta_N = -\frac{1}{D_{NN}} \sum_{i=0}^{N-1} D_{Ni}\Theta_i. \tag{A3}$$

The foregoing system of ordinary differential equations is solved by a semi-implicit third-order Runge–Kutta routine, STIFF3 [25], which proved very fast, giving extraordinarily good convergence. The combination of the aforementioned numerical procedures is very effective. For the problem at hand, the collocation solution is even more effective than the classical Dirichlet problem because there is no temperature discontinuity at the boundaries inasmuch as the interfacial temperature rises along with the substrate temperature. The wall temperature is determined with an accuracy of 0.1% with just five collocation points and five steps in time. The same accuracy with a finite-difference scheme (e.g. Crank–Nicolson) requires tens of thousands of points. Furthermore, the method converges exponentially and not linearly as finite differences do. Convergence starts approximately at the moment the wall temperature is raised by 0.5°C. Increasing the number of collocation points, N, may reduce this minimum requirement for the wall temperature to rise.